



Significance of carbonyl compounds to photochemical ozone formation in a coastal city (Shantou) in eastern China

Hengqing Shen^a, Yuhong Liu^a, Min Zhao^a, Juan Li^{b,*}, Yingnan Zhang^a, Juan Yang^a, Ying Jiang^a, Tianshu Chen^a, Miao Chen^b, Xianbing Huang^b, Chengliu Li^c, Danling Guo^c, Xiaoyan Sun^d, Likun Xue^{a,*}, Wenxing Wang^a

^a Environment Research Institute, Shandong University, Qingdao, Shandong 266237, China

^b Shantou Environmental Protection Monitoring Station, Shantou 515041, China

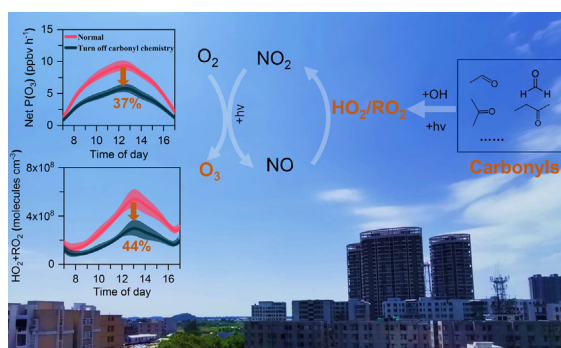
^c Shenzhen OnePoint Environmental Consultant Co., Ltd, Shenzhen 518000, China

^d Jinan Environmental Monitoring Center Station, Jinan, Shandong 250014, China

HIGHLIGHTS

- The significance of carbonyls to O₃ formation in urban Shantou was confirmed.
- O₃ formation was VOC-limited, and specifically most sensitive to carbonyls.
- Photolysis of carbonyls dominated the primary source of HO₂ and RO₂ radicals.
- Carbonyls accounted for 37% of the peak net production rate of O₃.

GRAPHICAL ABSTRACT



ARTICLE INFO

Article history:

Received 24 September 2020

Received in revised form 17 November 2020

Accepted 18 November 2020

Available online 24 December 2020

Editor: Philip K. Hopke

Keywords:

Carbonyl compounds

Ozone formation

Volatile organic compounds

Chemical box model

ABSTRACT

Carbonyl compounds are ubiquitous in the troposphere, yet their contributions to ambient ozone (O₃) formation have rarely been quantified in China. To better understand their roles in O₃ pollution, a field campaign was conducted at an urban site of Shantou, a coastal city in eastern China, during 7th–29th October 2019. Seven carbonyls were quantified (average ± standard deviation: 14.42 ± 3.05 ppbv), among which formaldehyde (4.12 ± 1.02 ppbv), acetaldehyde (1.57 ± 0.30 ppbv), acetone (7.55 ± 2.10 ppbv), and methyl ethyl ketone (0.94 ± 0.28 ppbv) were the most abundant species. Relative incremental reactivity (RIR) analysis indicated that O₃ formation in Shantou was VOC-limited, specifically most sensitive to carbonyls, and formaldehyde showed the largest RIR values in terms of individual species. Budgets of O₃ and RO_x (OH, HO₂, and RO₂) radicals were elucidated with a chemical box model. Carbonyls played a vital role in both the primary formation and recycling of the RO_x; more than 80% of the primary source of HO₂ and RO₂ came from photolysis of formaldehyde and other oxygenated VOCs. Zero-out sensitivity studies showed that the seven measured carbonyls accounted for 37% of the peak net O₃ production rate, mainly by affecting the concentrations of HO₂ and RO₂. These results highlight the significance of carbonyls, especially formaldehyde, to photochemical O₃ formation, and carbonyls should be paid more attention to mitigate the worsening O₃ pollution in China.

© 2020 Elsevier B.V. All rights reserved.

1. Introduction

Surface ozone (O₃) pollution has become a major challenge in air quality management in China. Since the Chinese government

* Corresponding authors.

E-mail addresses: lijuan10jli4@163.com (J. Li), xuelikun@sdu.edu.cn (L. Xue).

implemented the five-year plan for Clean Air Action in 2013, ambient concentrations of SO₂, NO₂, and PM_{2.5} have shown significant decreasing trends during 2013–2017 (Wang et al., 2020b; Zheng et al., 2018). However, at the same time, surface O₃ concentration levels have increased significantly in the urban areas of eastern China (Li et al., 2019; Lu et al., 2018), which is the region with the largest population and the fastest economic growth of China. Elevated surface O₃ concentrations exert severe adverse effects on public health, and the estimated annual mortality attributable to surface O₃ exposure is over 150,000 deaths in China (Malley et al., 2017). O₃ pollution is also detrimental to key staple crop yields, reducing the yields of wheat, soybean, and maize by up to 15%, and is threatening global food security (Avnery et al., 2011; Mills et al., 2018).

Surface O₃ is generated by the oxidation of volatile organic compounds (VOCs) in the presence of nitrogen oxides (NO_x = NO + NO₂) and sunlight. The key step of O₃ formation is the oxidation of NO to NO₂ by peroxy radicals, e.g., hydroperoxy (HO₂) and organic peroxy (RO₂) radicals. The photochemical oxidation of VOCs that perturbs HO₂ and RO₂ radicals will directly affect O₃ formation (Li et al., 2018b; Li et al., 2019; Yang et al., 2018). Many previous studies have established that O₃ formation in urban areas is generally VOC-limited (Li et al., 2020; Lu et al., 2019a; Shao et al., 2009; Wang et al., 2017b; Zhang et al., 2020a), i.e., mitigation of VOC emissions will suppress O₃ formation, while a small amount of reduction in NO_x emissions may increase O₃ concentration at NO_x-saturated regimes. However, the reactivities (e.g., OH reactivity, L_{OH}) and O₃ formation potentials of different VOCs vary widely (Carter, 1994; Li et al., 2020; Russell et al., 1995). Therefore, it is critical to rank the contributions of different VOCs to O₃ formation to regulate O₃ pollution effectively.

Carbonyl compounds (including aldehydes and ketones) are important components of oxygenated volatile organic compounds (OVOCs) from both primary and secondary sources and play important roles in atmospheric chemistry and urban air quality (Calvert et al., 2011; Mellouki et al., 2015; Shen et al., 2018). The photolysis of carbonyls is an important source of peroxy radicals in the atmosphere, contributing to up to 80% of primary sources of HO₂ and RO₂ radicals (Calvert et al., 2011; Xue et al., 2016b; Yang et al., 2018), which will undoubtedly further affect ambient O₃ formation (Edwards et al., 2014; Wang et al., 2017a; Zhang et al., 2019). However, most of the previous evaluations for the roles of VOCs in O₃ formation focused on hydrocarbons in China (Li et al., 2020; Shao et al., 2009; Wu et al., 2017), and the contributions of carbonyls have rarely been quantified, partly due to the lack of observation data. Several recent studies indicated the important potential contributions of carbonyls to atmospheric oxidizing capacity and O₃ concentrations in the oil and gas basin areas (Chen et al., 2020;

Edwards et al., 2014). Nonetheless, there is still little effort to comprehensively explore the roles of carbonyls in urban O₃ formation and quantify their relative contributions compared with other VOCs in China. This is crucial to developing effective O₃ control strategies in urban areas, usually with high concentrations of carbonyls (Qian et al., 2019; Rao et al., 2016; Salthammer, 2013; Wang et al., 2017a).

Shantou is one of the earliest five special economic zones in China and is between China's most economically developed Yangtze River Delta (YRD) and Pearl River Delta (PRD) regions, where anthropogenic emissions of air pollutants, including non-methane hydrocarbons (NMHCs), are high (see Fig. 1). Eastern China, including Shantou, is experiencing severe air pollution in recent years (Lu et al., 2018; Zhang and Cao, 2015). However, studies on air pollution, especially O₃ pollution in Shantou, are still lacking. To better understand the roles of carbonyls in urban O₃ formation, we conducted simultaneous measurements of 56 NMHCs, seven carbonyls, O₃, and related parameters at an urban site of Shantou in October 2019. The characteristics of carbonyls and their contributions to O₃ formation were investigated and compared with other VOCs. Besides, we identified the roles of carbonyls in O₃ formation and radical budgets with the aid of an observation-based chemical box model. Results show that carbonyls play a crucial role in photochemical O₃ formation in Shantou and must be considered to regulate O₃ pollution effectively.

2. Methods

2.1. Measurement methods

The field campaign was conducted at an urban site of Shantou (Haojiang station, 23.28° N, 116.72° E, about 10 m above sea level, Fig. 1) from 7 October to 29 October 2019. This observation site is located on the campus of a middle school, away from the main road, but there are several small lanes around it. Residential buildings surround the observation point, and there is no significant industrial pollution nearby. The instruments were located on the roof of a building (~16 m above the ground). Samples of carbonyls were collected using a two-channel sampler (TH-110E, Wuhan Tianhong, China). Ambient air was drawn through 2,4-dinitrophenylhydrazine (DNPH) cartridges (Waters, USA) with an ozone-scrubber cartridge (Waters, USA) filled with potassium iodide (KI) being connected to its front to eliminate O₃ interference. The samples were generally collected from 7:00 to 17:00 local time (LT) with a flow rate of 0.5 L min⁻¹ and a duration of 2 h. On normal days, there was at least one sample being collected from 13:00 to 15:00 LT when O₃ concentrations increased to the highest (Fig. S1). To better capture the effects of carbonyls on photochemical O₃

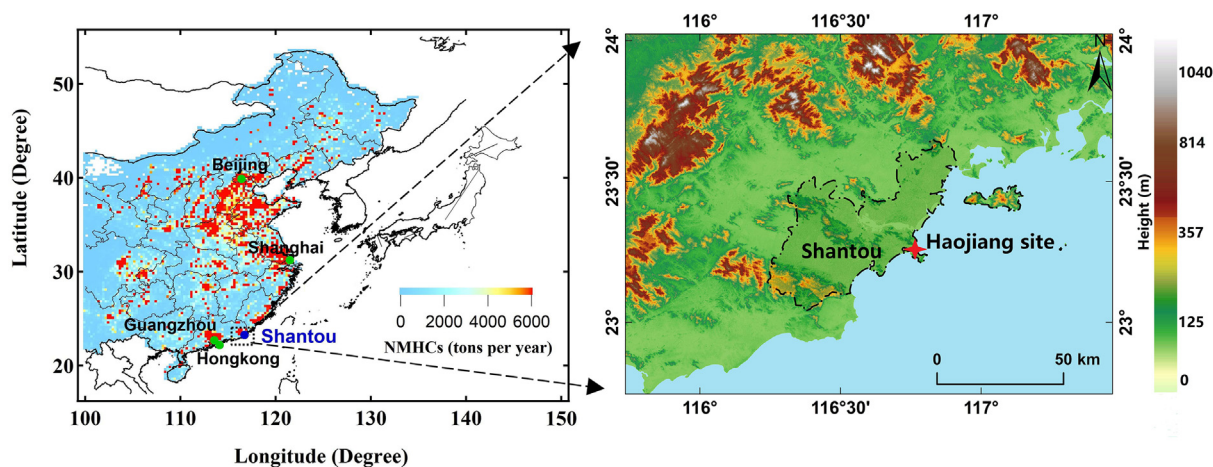


Fig. 1. Maps showing the location of Shantou, a coastal city in eastern China. The data of anthropogenic NMHCs emissions in 2016 was obtained from the MEIC (the Multi-resolution Emission Inventory for China, <http://www.meicmodel.org>), and the geographical data was obtained from <https://search.asf.alaska.edu>.

formation and facilitate model simulations, five samples were collected on days with predicted O₃ pollution episodes (five samples were collected per day on October 9–10 and October 18–21). Parallel samples were collected using the other channel of the sampler, and field blank samples were collected by placing the cartridges near the sampling inlet for the same duration. A total of 62 samples were obtained, including 46 ambient samples, ten parallel samples, and six blank samples.

The carbonyls in the samples would react with the DNPH coated on silica gel and be catalyzed by strong acid to produce stable and colored hydrazone derivatives. The DNPH cartridges were eluted with 5 mL of acetonitrile (*LC grade, Merck, Germany*), and then analyzed by high performance liquid chromatography (HPLC, *PerkinElmer Series 2000*) and detected with an ultraviolet detector (detecting wavelength was 360 nm). LC separation of carbonyls was conducted by using a mixture of acetonitrile and water as the mobile phase. The gradient program was as follows: constant 60% acetonitrile and 40% water during 0–20 min, then linearly increased to 100% acetonitrile in 20–30 min; the content of acetonitrile decreased to 60% in 30–32 min and kept constant until 40 min. An *Agilent Zorbax Eclipse XDB-C18* column (250 mm × 4.6 mm × 5 μm) was used as the analytical column, and the column temperature was set to 25 °C. The flow rate of the mobile phase was 1.2 mL min⁻¹, and the injection volume was 20 μL. Carbonyls were identified and quantified by the liquid standard solution of 13 carbonyls (i.e., formaldehyde, acetaldehyde, acetone, acrolein, propionaldehyde, crotonaldehyde, methacrolein, methyl ethyl ketone, butanal, benzaldehyde, pentanal, p-tolualdehyde, and hexanal). Their retention times were provided in the supporting information, and the limits of detection of all these 13 carbonyls were below 0.05 ppbv. In the present study, only seven carbonyl compounds, i.e., formaldehyde, acetaldehyde, acetone, propionaldehyde, methyl ethyl ketone (MEK), benzaldehyde, and hexanal, were detected from the ambient samples, and the other six carbonyl compounds were below the detection limits.

Ambient VOCs were monitored by online gas chromatography–mass spectrometry (GC–MS; *TH300B, Wuhan Tianhong, China*). This system automatically collected air samples every 1 h at a flow rate of 40 mL min⁻¹ and a sampling time of 10 min. The analytical instrument was *Agilent GC:8860/MS:5977B*. After TH-300B pretreatment and ultra-low temperature trapped heat desorption, the sample was divided into two paths. One path was detected by flame ionization detector (FID) (C₂–C₅ compounds) after passing through the *DM-PLOT Alumina/Na₂SO₄* column (30 m × 320 μm × 5 μm), and the other path was detected by MS detector (C₆–C₁₂ compounds) after passing through the *Agilent DB624* column (60 m × 250 μm × 1.4 μm). The limits of detection of all measured VOCs were below 0.01 ppbv. Ambient concentrations of O₃, NO_x, SO₂, and CO were measured by widely-used commercial analyzers of Model 49i, Model 42i, Model 43i, and Model 48i (*Thermo Scientific, USA*), respectively. The meteorological parameters were obtained from the local meteorological bureau.

2.2. Observation-based chemical box model

The Observation-Based Model for investigating Atmospheric Oxidative Capacity and Photochemistry (OBM-AOCP) has been extensively used to simulate O₃ formation and analyze radical budgets (Chen et al., 2020; Xue et al., 2016a; Xue et al., 2014; Yang et al., 2018). It is based on the latest version of the Master Chemical Mechanism (MCM v3.3.1, <http://mcm.york.ac.uk>) (Bloss et al., 2005; Jenkin et al., 1997; Jenkin et al., 2003; Jenkin et al., 2015; Saunders et al., 2003). In addition to the existing reactions, several heterogeneous reactions and physical processes such as dry deposition and dilution mixing within the boundary layer are also included. The detailed descriptions can be found in the previous studies (Xue et al., 2016b; Xue et al., 2014).

In this study, the model was constrained by the measured VOCs, carbonyls, O₃, NO_x, SO₂, CO, and physical parameters (i.e., water vapor concentration and temperature), and the unavailable nighttime data of carbonyls were interpolated using the multiple linear regressions with

CO and O₃ (Yang et al., 2018). The photolysis frequencies were obtained from the Tropospheric Ultraviolet and Visible (TUV, v5.3.1) model, and those not included in the TUV model were calculated by the solar zenith angle (<http://mcm.york.ac.uk/parameters/photolysis.htm>) (Saunders et al., 2003). The dry deposition was set according to previous parameters (Xue et al., 2014), while the dry deposition velocity of O₃ was derived from the latest study (Clifton et al., 2020). We mainly focus on the continuous four days (18 October–21 October) with multiple samples of carbonyls being collected in the model simulation. This period includes the day with the highest O₃ concentration during the observation (19 October, with maximum hourly O₃ concentration of 92.4 ppbv). The model was pre-run for three days to reach the steady-state of unconstrained species.

Detailed calculation processes of O₃ and radical budgets have also been described elsewhere (Chen et al., 2020; Xue et al., 2016b; Xue et al., 2014; Xue et al., 2013). The primary sources of OH, HO₂, and RO₂ considered were the photolysis reactions of O₃, HONO, formaldehyde (HCHO), and other OVOCs, as well as reactions of VOCs with O₃ and NO₃ radical, and the recycling processes and important sinks of these radicals were also considered (Chen et al., 2020; Xue et al., 2016b). The O₃ production rate (P(O₃)) was calculated as the sum of reaction rates for HO₂ + NO and RO₂ + NO (Eq. 1), assuming that the yield of NO₂ from the RO₂ + NO reaction was 1 (Lu et al., 2010). The O₃ loss rate (L(O₃)) was calculated as the sum of the reaction rates for O₃ photolysis (represented as k_{O(1D)+H₂O}[O(1D)][H₂O]), O₃ + OH, O₃ + HO₂, O₃ + VOCs, NO₂ + OH, NO₂ + RO₂, and NO₃ + VOCs (Eq. 2) (Chen et al., 2020). The net O₃ production rate was determined from the difference between P(O₃) and L(O₃) (Eq. 3).

$$P(O_3) = k_{HO_2+NO}[HO_2][NO] + \sum k_{RO_2+NO}[RO_2][NO] \quad (1)$$

$$\begin{aligned} L(O_3) = & k_{O(1D)+H_2O}[O(1D)][H_2O] + k_{O_3+OH}[O_3][OH] \\ & + k_{O_3+HO_2}[O_3][HO_2] + \sum k_{O_3+VOCs}[O_3][VOCs] \\ & + k_{NO_2+OH}[NO_2][OH] + \sum k_{RO_2+NO_2}[RO_2][NO_2] \\ & + 2 \sum k_{NO_3+VOCs}[NO_3][VOCs] \end{aligned} \quad (2)$$

$$\text{Net } P(O_3) = P(O_3) - L(O_3) \quad (3)$$

3. Results and discussion

3.1. General characteristics

The concentration levels and OH reactivities (L_{OH}) of the measured VOC species are summarized in Table 1, and time series and descriptive statistics of other trace gases and meteorological parameters are provided in the supporting information. The hourly averaged O₃ level (±standard deviation, SD) was 54.8 ± 13.8 ppbv during this observation. The maximum daily 8 h O₃ of four days exceeded 160 μg m⁻³ (about 75 ppbv) (China's Grade II National Ambient Air Quality Standard), and the maximum hourly value was up to 92.4 ppbv. This level was comparable to those reported in polluted North China Plain (NCP) and PRD regions (Hu et al., 2016; Li et al., 2019; Lu et al., 2018). Despite as an urban site, the concentrations of CO, SO₂, NO, and NO₂ were not very high compared to some other polluted urban areas (Hu et al., 2016; Wang et al., 2017a; Wang et al., 2020a), with average levels (±SD) of 491.4 ± 116.7 ppbv, 2.3 ± 0.6 ppbv, 0.9 ± 0.6 ppbv, and 5.2 ± 2.0 ppbv, respectively. The average temperature, relative humidity (RH), PM_{2.5}, and wind speed (±SD) were 24.9 ± 2.1 °C, 53.2% ± 10.1%, 23.1 ± 7.8 μg m⁻³, and 2.3 ± 1.2 m s⁻¹, respectively. Overall, the data revealed a moderate pollution

Table 1
Descriptive statistics of concentrations and OH reactivities of the measured VOCs during this observation.

	Species	Average (ppbv)	Range (ppbv)	L_{OH} (s^{-1})	
Alkanes	Ethane	1.92 ± 0.65	0.79–4.17	0.012 ± 0.004	
	Propane	3.74 ± 2.10	0.86–15.71	0.098 ± 0.055	
	i-Butane	0.97 ± 0.54	0.25–3.49	0.018 ± 0.010	
	n-Butane	1.62 ± 0.88	0.32–5.96	0.094 ± 0.051	
	n-Pentane	0.45 ± 0.33	0.14–3.63	0.015 ± 0.011	
	i-Pentane	1.24 ± 0.67	0.33–4.60	0.113 ± 0.061	
	Cyclopentane	0.99 ± 1.31	0.04–6.44	0.059 ± 0.078	
	2,2-Dimethylbutane	0.06 ± 0.04	0.01–0.24	0.004 ± 0.002	
	2-Methylpentane	0.33 ± 0.26	0.08–2.08	0.043 ± 0.034	
	2,3-Dimethylbutane	0.35 ± 0.27	0.08–2.16	0.017 ± 0.013	
	3-Methylpentane	0.28 ± 0.20	0.06–1.59	0.037 ± 0.027	
	Cyclohexane	0.06 ± 0.07	0.01–0.88	0.003 ± 0.004	
	2-Methylhexane	0.09 ± 0.07	0.02–0.66	0.014 ± 0.011	
	2,3-Dimethylpentane	0.08 ± 0.07	0.02–0.66	0.011 ± 0.009	
	3-Methylhexane	0.18 ± 0.24	0.02–3.02	0.031 ± 0.042	
	2,2,4-Trimethylpentane	0.08 ± 0.06	0.02–0.64	0.010 ± 0.008	
	n-Heptane	0.16 ± 0.13	0.04–0.70	0.009 ± 0.008	
	Methylcyclohexane	0.06 ± 0.13	0.01–1.42	0.003 ± 0.008	
	2,3,4-Trimethylpentane	0.04 ± 0.03	0.01–0.35	0.005 ± 0.004	
	2-Methylheptane	0.04 ± 0.15	0.01–1.57	0.003 ± 0.011	
	n-Hexane	0.22 ± 0.14	0.05–1.05	0.010 ± 0.006	
	2,4-Dimethylpentane	0.26 ± 0.38	0.03–2.23	0.034 ± 0.049	
	Methylcyclopentane	0.08 ± 0.05	0.02–0.49	0.005 ± 0.003	
	3-Methylheptane	0.04 ± 0.14	0.01–1.49	0.003 ± 0.010	
n-Octane	0.11 ± 0.23	0.02–2.82	0.008 ± 0.017		
n-Nonane	0.05 ± 0.07	0.01–1.35	0.004 ± 0.006		
n-Decane	0.05 ± 0.08	0.01–1.26	0.004 ± 0.007		
n-Undecane	0.07 ± 0.08	0.05–0.68	0.022 ± 0.025		
n-Dodecane	0.18 ± 0.07	0.10–0.56	0.061 ± 0.024		
Total	13.53 ± 6.31	4.81–42.37	0.750 ± 0.598		
Alkenes	Ethylene	1.16 ± 1.10	0.13–7.43	0.226 ± 0.215	
	Propylene	0.46 ± 0.71	0.03–5.01	0.329 ± 0.505	
	1-Butene	0.20 ± 0.20	0.03–0.99	0.157 ± 0.155	
	Cis-2-butene	0.08 ± 0.05	0.03–0.25	0.107 ± 0.066	
	Trans-2-butene	0.12 ± 0.07	0.03–0.36	0.191 ± 0.114	
	1-Pentene	0.12 ± 0.17	0.02–1.01	0.093 ± 0.133	
	Trans-2-pentene	0.08 ± 0.12	0.01–0.75	0.132 ± 0.190	
	Isoprene	0.18 ± 0.23	0.10–1.32	0.444 ± 0.556	
	Cis-2-pentene	0.03 ± 0.01	0.02–0.07	0.042 ± 0.021	
	1-Hexene	0.16 ± 0.21	0.01–1.12	0.142 ± 0.189	
	Total	2.05 ± 2.48	0.20–17.12	1.863 ± 2.146	
	Acetylene	Acetylene	1.28 ± 0.86	0.26–5.75	0.020 ± 0.020
	Aromatics	Benzene	0.44 ± 0.23	0.13–1.71	0.013 ± 0.007
Toluene		1.01 ± 0.79	0.13–7.05	0.140 ± 0.109	
Ethylbenzene		0.22 ± 0.17	0.04–1.43	0.038 ± 0.029	
Styrene		0.10 ± 0.10	0.01–0.38	0.139 ± 0.147	
i-Propylbenzene		0.03 ± 0.01	0.02–0.12	0.005 ± 0.002	
n-Propylbenzene		0.03 ± 0.02	0.01–0.26	0.004 ± 0.003	
2-Ethyltoluene		0.03 ± 0.03	0.01–0.29	0.009 ± 0.008	
1,3,5-Trimethylbenzene		0.04 ± 0.04	0.02–0.54	0.054 ± 0.052	
1,2,4-Trimethylbenzene		0.15 ± 0.11	0.03–1.01	0.117 ± 0.087	
1,2,3-Trimethylbenzene		0.04 ± 0.03	0.01–0.41	0.028 ± 0.025	
1,3-Diethylbenzene		0.02 ± 0.01	0.01–0.07	0.014 ± 0.006	
1,4-Diethylbenzene		0.05 ± 0.07	0.02–0.83	0.018 ± 0.026	
4-Ethyltoluene		0.04 ± 0.03	0.01–0.33	0.012 ± 0.009	
3-Ethyltoluene		0.07 ± 0.06	0.02–0.69	0.031 ± 0.028	
o-Xylene		0.22 ± 0.22	0.04–2.49	0.075 ± 0.073	
m/p-Xylene		0.55 ± 0.55	0.07–6.12	0.314 ± 0.310	
Total		2.95 ± 1.88	0.71–14.43	1.012 ± 0.921	
Carbonyls		Formaldehyde	4.12 ± 1.02	2.56–7.31	0.875 ± 0.217
		Acetaldehyde	1.57 ± 0.30	0.93–2.52	0.578 ± 0.110
	Acetone	7.55 ± 2.10	4.32–14.06	0.033 ± 0.009	
	Methyl ethyl ketone	0.94 ± 0.28	0.64–1.79	0.026 ± 0.008	
	Propionaldehyde	0.12 ± 0.03	0.07–0.27	0.056 ± 0.014	
	Benzaldehyde	0.08 ± 0.03	0.04–0.15	0.025 ± 0.009	
	Hexanal	0.05 ± 0.01	0.03–0.08	0.035 ± 0.007	
	Total	14.42 ± 3.05	9.71–22.78	1.627 ± 0.374	

situation of O_3 and O_3 precursors during the measurement period in urban Shantou.

For carbonyl compounds, acetone showed the highest level with an average value of 7.55 ± 2.10 ppbv, accounting for, on average, 52% of the measured total carbonyls. The high acetone levels were mainly

due to its large anthropogenic emissions and relatively low reactivity compared to other carbonyls (Qian et al., 2019; Wollenhaupt et al., 2000; Zhu et al., 2019). The levels of formaldehyde, acetaldehyde, and MEK were also relatively high, accounting for 29% (4.12 ± 1.02 ppbv), 11% (1.57 ± 0.30 ppbv), and 6% (0.94 ± 0.28 ppbv), respectively, of

total measured carbonyls. The proportions of propionaldehyde, benzaldehyde, and hexanal were minor (less than 1%). Such carbonyl levels were observed in some other urban areas in China, and over 10 ppbv of formaldehyde was observed before in the NCP and YRD regions (Rao et al., 2016; Zhang et al., 2019).

The levels of the measured total VOCs (including seven carbonyls and 56 NMHCs), with an average value of 34.21 ± 13.02 ppbv, were also comparable to the previously measured results in other urban areas such as Beijing and Shanghai (Li et al., 2015; Wu et al., 2016; Zhang et al., 2020b). Carbonyls constituted the largest portion of the measured total VOCs (42%, 14.42 ± 3.05 ppbv), followed by alkanes (39%, 13.53 ± 6.31 ppbv), aromatics (9%, 2.95 ± 1.88 ppbv), alkenes (6%, 2.05 ± 2.48 ppbv), and acetylene (4%, 1.28 ± 0.86 ppbv). Carbonyls were the second-largest contributor to L_{OH} of the measured VOCs, accounting for 31% ($1.6 \pm 4.1 \text{ s}^{-1}$) of the total ($5.3 \pm 4.1 \text{ s}^{-1}$). These indicated that carbonyls were important components of VOCs in the urban atmosphere of Shantou. It should be noted that only daytime data were measured for carbonyls, while there are continuous hourly data of day and night for NMHCs.

Figs. 2 and 3 present the average diurnal variations of major trace gases (including measured seven carbonyls and grouped VOCs) and meteorological parameters during this observation. These well-defined diurnal variations reflected the evolution of the boundary layer, primary emissions, and atmospheric photochemistry. O_3 exhibited a unimodal distribution, rapidly increasing after the sunrise, reaching a peak at 15:00 LT, and then continuously decreasing until the next morning. The rapid morning rise in O_3 was caused by entrainment of O_3 -rich air from the residual layer aloft (Galbally and Roy, 1980; Garland and Derwent, 1979; Karlsson et al., 2017). Diurnal variations of NO_x , CO, and SO_2 all showed a peak in the morning rush hour between 7:00 and 9:00 LT, and NO_2 and CO also showed a smaller peak between 18:00 and 19:00 LT. The diurnal variations of alkanes, alkenes, acetylene, and aromatics showed similar variations with those anthropogenic inorganic gases, with two peaks occurring at 9:00 and 19:00 LT, respectively. These diurnal variation patterns suggest that vehicle exhaust may significantly influence the emission of anthropogenic pollutants at this site and should be a major source of the measured VOCs.

In comparison, the diurnal variations of several carbonyls were different from the hydrocarbons. As with hydrocarbons, the highest levels of propionaldehyde, benzaldehyde, and hexanal appeared at 7:00–9:00 LT, implying their potentially similar sources, e.g., vehicle exhaust or the entrainment from residual layer aloft like O_3 (Karlsson et al., 2017; Qian

et al., 2019). The highest levels of acetaldehyde and acetone also appeared before noon, while later than the previous three (at 9:00–11:00 LT). For formaldehyde, its average levels increased in the daytime and peaked in the 13:00–15:00 LT when O_3 levels also peaked. Formaldehyde, acetaldehyde, and acetone all maintained relatively high levels throughout the daytime. The diurnal variations of these three carbonyls might show the combined effect of primary emissions and secondary formation. The high MEK level at noon may reflect a strong marine source (sea-land breeze) (Brewer et al., 2020). Overall, the diurnal variations of these carbonyls implied that both primary and secondary source might contribute to these measured carbonyls in Shantou (Chen et al., 2014; Grosjean et al., 2001; Nogueira et al., 2015; Qian et al., 2019), especially for formaldehyde, acetaldehyde, and acetone. It should be noted that the entrainment of the residual layer aloft may also significantly influence the diurnal variations of these carbonyls.

3.2. Ozone-precursor relationships

The O_3 -precursor relationship is diagnosed by relative incremental reactivity (RIR) calculations based on the simulations of the OBM-AOCP. The performance of the model on O_3 simulation was evaluated in the supporting information. Here, RIR is defined as the change of net O_3 production rate induced by the change in concentrations of its precursors (i.e., CO, NO_x , and specific VOCs/group of VOCs). RIR values can be calculated by Eq. 4:

$$RIR(X) = \frac{[\text{Net } P_{O_3}(X) - \text{Net } P_{O_3}(X - \Delta X)] / (\text{Net } P_{O_3}(X))}{\Delta X / X} \quad (4)$$

where net P_{O_3} is the net production rate of O_3 simulated by the model, X represents the concentration of either a specific precursor or a group of VOCs, ΔX is the hypothetical change of the concentration of X (10% was adopted in this study). The positive values of RIR indicate the reduction of its precursor inhibits O_3 formation, and negative values indicate the reduction of its precursor enhances O_3 formation.

Fig. 4 shows the model-calculated RIR values for different groups of VOCs, NO_x , and CO, as well as the top 10 VOC species. The RIR values of all the measured groups of VOCs and CO were positive, while that of NO_x was negative (-0.16). This suggests that O_3 formation in Shantou was mainly VOC-limited, i.e., the reduction of VOCs could lead to O_3 reduction, while a 10% reduction of NO_x might lead to an increase of O_3 to a certain degree. The RIR value of carbonyls was the largest (0.37)

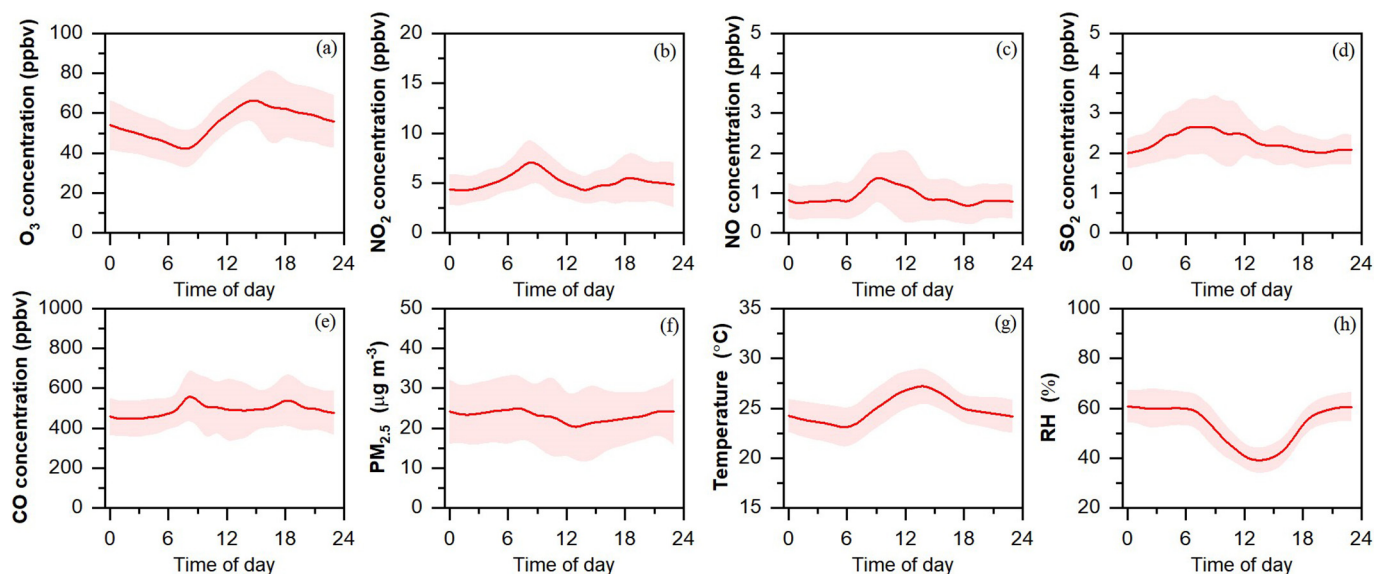


Fig. 2. Diurnal variations of major trace gases, $PM_{2.5}$, and meteorological parameters during the observation. The error bar indicates the standard deviation of the mean.

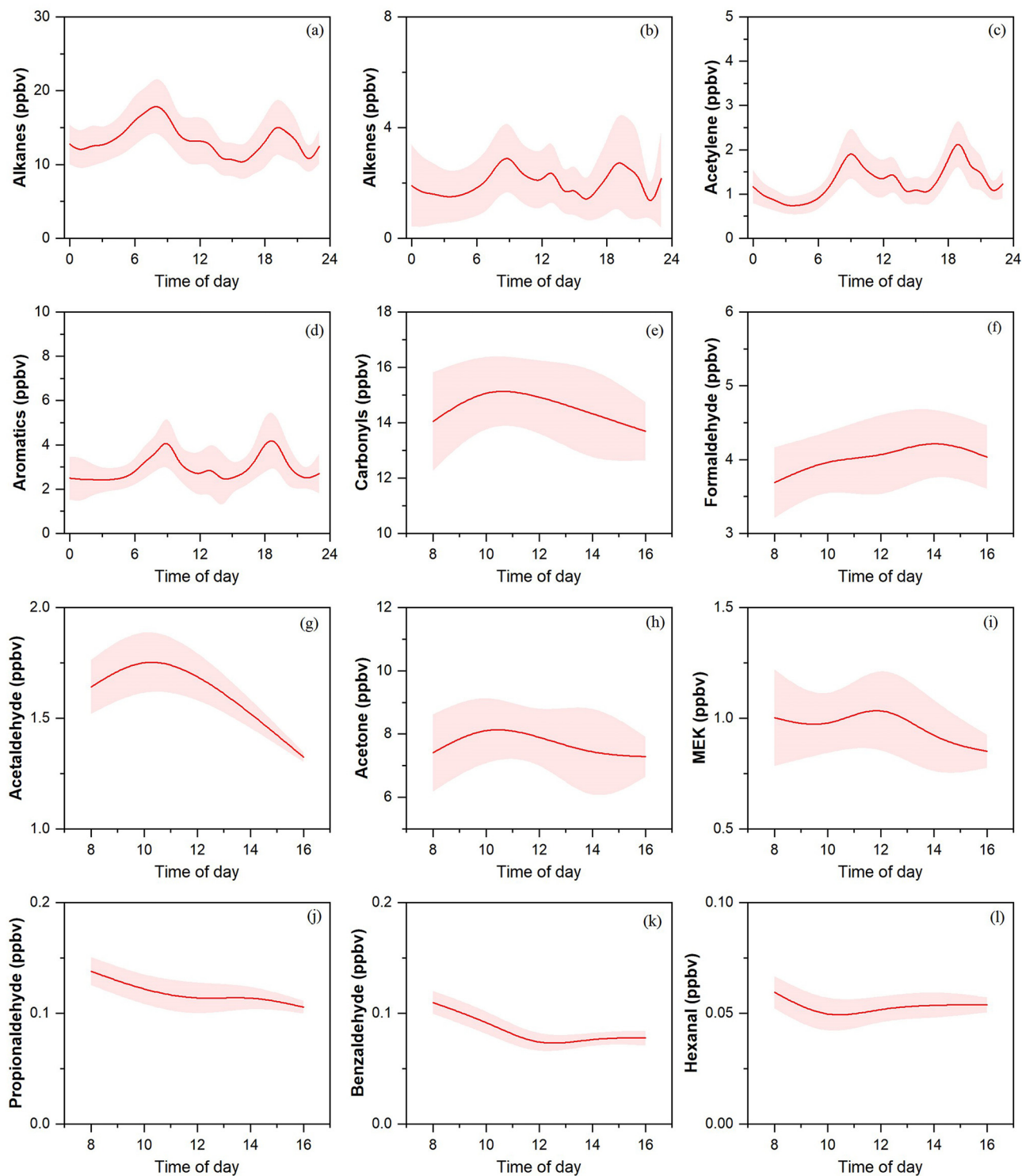


Fig. 3. Diurnal variations of major VOC groups and seven individual carbonyls. It should be noted that only daytime (7:00–17:00 LT) data were measured for carbonyls. The error bar indicates half of the standard deviation of the mean.

among the tested precursors, similar to that reported in urban Beijing (Yang et al., 2018). Aromatics showed a slightly lower RIR value (0.36) than carbonyls but was also much higher than those of alkanes and alkenes (0.07 and 0.10, respectively). As for the individual species, formaldehyde showed the largest RIR (0.21), followed by m/p-xylene (0.12), acetaldehyde (0.11), and toluene (0.05). Other carbonyls among the top 10 VOCs were acetone and MEK, but their RIR values were relatively minor (both were 0.01) compared to formaldehyde. This demonstrated

the dominant roles of carbonyls, especially formaldehyde and acetaldehyde, in O_3 formation in urban Shantou.

3.3. Roles of carbonyls in ozone and radical budgets

We further explored the roles of carbonyls in O_3 formation through detailed chemical budget analyses of O_3 and RO_x (OH, HO_2 , and RO_2). Daytime (7:00–17:00 LT) averaged $P(O_3)$ (defined as the sum of

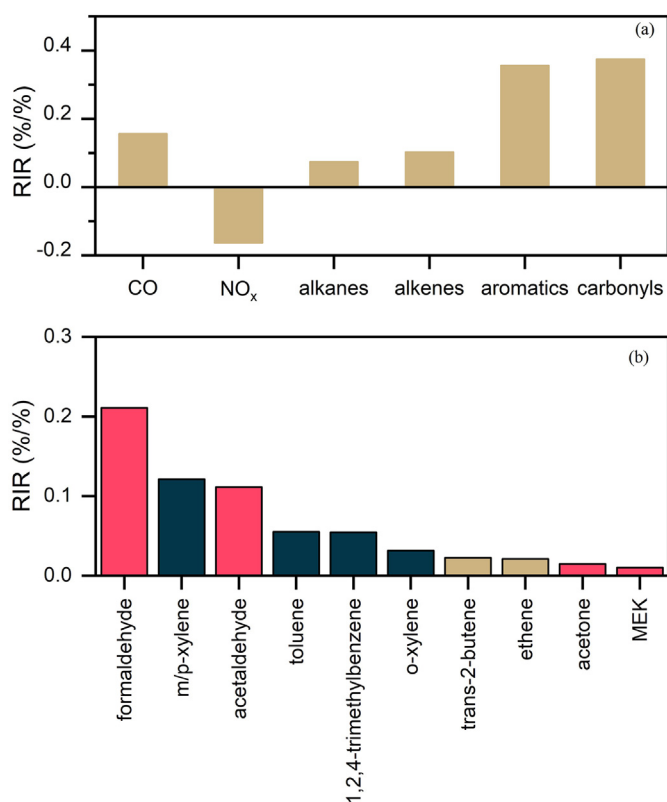


Fig. 4. (a) The RIR values for different O_3 precursors and (b) the RIR values for the top 10 VOC species. The data were the averages of daytime (7:00–17:00 LT) values. The colors of red, dark blue, and brown in (b) represent carbonyl compounds, aromatics, and alkenes, respectively.

reaction rates of HO_2+NO and RO_2+NO) was 7.6 ± 0.5 ppbv h^{-1} , with a maximum value of 11.5 ± 0.9 ppbv h^{-1} occurring at 13:00 LT during the modeled four days episodes (Fig. 5). This level was within the previously reported range (Farmer et al., 2011; Ojha et al., 2012; Vermeuel et al., 2019), but slightly lower than that of the heavily polluted areas in China (Chen et al., 2020; Liu et al., 2012; Lu et al., 2019b; Lu et al., 2010). The proportions of HO_2+NO and RO_2+NO channels were 58% and 42%, respectively. Therefore, any process that perturbs HO_2 and RO_2 radicals will directly affect O_3 formation. The $L(O_3)$ was relatively small, mainly through NO_2+OH (48%), NO_2+RO_2 (17%), and O_3 photolysis (14%) channels. The daytime averaged (\pm SD) net $P(O_3)$ was 6.2 ± 0.4 ppbv h^{-1} , with a maximum value of 9.5 ± 0.8 ppbv h^{-1} at 13:00 LT.

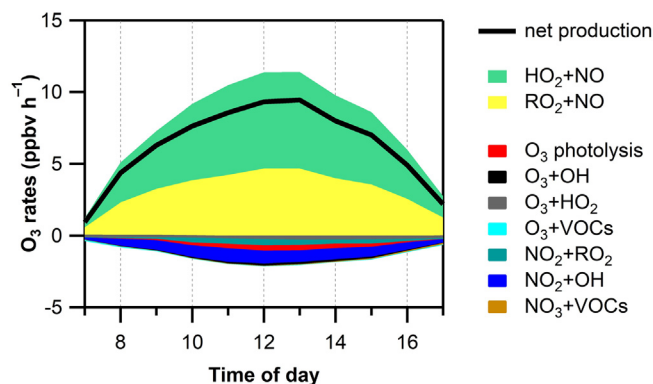


Fig. 5. Daytime (7:00–17:00 LT) averaged O_3 chemical budget during the selected episode (18 October–21 October).

To better understand the roles of carbonyls, we elucidated the budgets of major atmospheric radicals (OH , HO_2 , and RO_2) (Fig. 6) based on the model and particularly focused on the roles of carbonyls on their primary formation (Fig. 7). The radical recycling was the dominant source of these radicals, accounting for 89%, 86%, and 85% of the total considered sources for OH , HO_2 , and RO_2 , respectively. The channels to account for the largest proportion were HO_2+NO for OH source (87%), $OH+VOCs/CO$ for HO_2 source (49%), and $OH+VOCs$ for RO_2 source (75%), respectively. For the termination reactions, RO_x+NO_x (e.g., $OH+NO_2$, and RO_x+NO/NO_2) was the most important channel, while the contributions of the cross-reactions of radicals (e.g., HO_2+HO_2 and HO_2+RO_2) were minor. This was consistent with previous studies in polluted urban and suburban areas in China (Tan et al., 2019b; Tan et al., 2018).

In terms of the primary formation, O_3 photolysis was the dominant source of OH radicals, with an average value of 0.37 ppbv h^{-1} and a maximum value of 0.74 ppbv h^{-1} . HONO photolysis was also an important source, mainly before noon (up to 0.22 ppbv h^{-1}). It should be noted that the HONO concentration was not constrained, and only the gas-phase source was considered in the model. So the contribution of HONO photolysis to OH source may be underestimated (Li et al., 2018a; Yang et al., 2021). The contributions of OVOCs photolysis and reactions of O_3 with VOCs were relatively minor in Shantou. For HO_2 radicals, the photolysis of formaldehyde contributed 57% (0.38 ppbv h^{-1}) of its primary source. This proportion was similar to that reported in urban Beijing (Yang et al., 2018), despite that the absolute value was lower in Shantou (about one ppbv h^{-1} in Beijing). Photolysis of other OVOCs (mainly carbonyls) also had large contributions, with a daytime averaged proportion of 39% (0.26 ppbv h^{-1}). This suggests that carbonyls were the dominant contributors to primary HO_2 radicals. For RO_2 radicals, the photolysis of OVOCs was the largest contributor in the daytime, accounting for 88% (0.30 ppbv h^{-1}) of primary RO_2 production. These results highlighted the crucial role of OVOCs in the primary HO_2 and RO_2 formation in the urban atmosphere of Shantou, which will further affect O_3 formation (Edwards et al., 2014).

We conducted a zero-out sensitivity simulation constraining the mixing ratios of all the measured carbonyls to zero to quantify the role of carbonyls in O_3 formation. Under this condition, there would be no photochemistry of carbonyls in the model. The results are shown in Fig. 8. The change of RO_x budgets and the effects of different reduction ratios of carbonyls from 0% to 100% on net $P(O_3)$ are provided in Figs. S4 and S5, respectively. It can be seen clearly from Fig. 8a that net $P(O_3)$ decreased significantly without carbonyl chemistry, the daytime averaged net $P(O_3)$ decreased by 40% (from 6.2 ppbv h^{-1} to 3.7 ppbv h^{-1}), and the maximum net $P(O_3)$ decreased by 37% (from 9.4 ppbv h^{-1} to 5.9 ppbv h^{-1}). Fig. 8b–d shows the modeled concentration variations of OH , HO_2 , and RO_2 with and without photochemistry of carbonyls. Their modeled concentration levels and diurnal variations were comparable with previous field observations (Lu et al., 2012; Tan et al., 2019a). Without considering the photochemistry of carbonyls, peak levels for OH , HO_2 , and RO_2 radicals would decrease by 18%, 44%, and 46%, respectively, and average levels would decrease by 22%, 44%, and 45%, respectively. This large decrease was consistent with the decrease of net $P(O_3)$ and proved that carbonyls exert a strong influence on urban O_3 formation by affecting HO_2 and RO_2 , through not only their primary formation but also radical recycling (Fig. S4). The results in the present study underline the key role of carbonyls in the atmospheric oxidation capacity and O_3 formation, and highlight the urgent need to take carbonyls into consideration when establishing science-based control strategies for O_3 pollution in eastern China.

4. Summary

The significance of carbonyls to photochemical O_3 formation was explored through a field campaign conducted at an urban site of Shantou, eastern China. Seven carbonyls were quantified (formaldehyde,

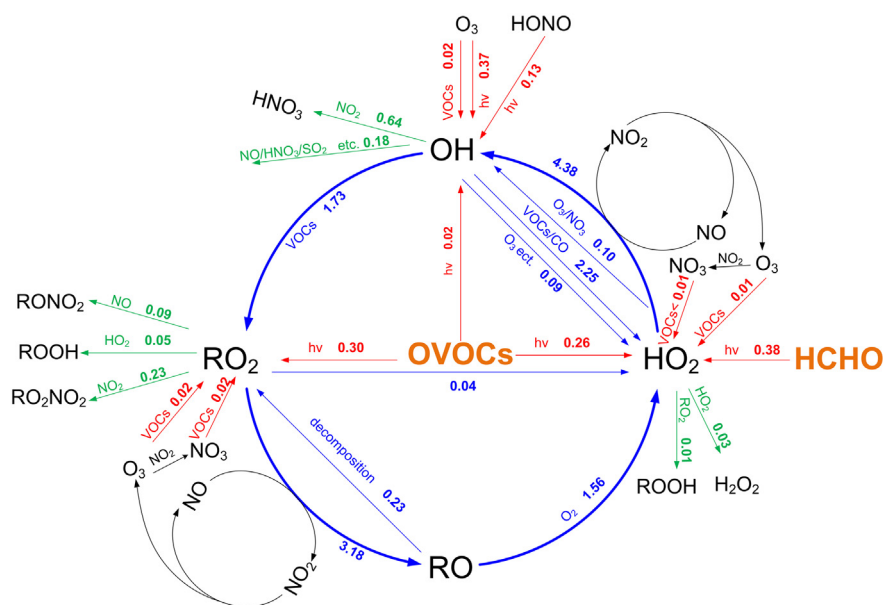


Fig. 6. Daytime (7:00–17:00 LT) averaged RO_x radical budget simulated by the model. The red, green, and blue lines indicate the primary production, destruction, and recycling pathways, respectively. Unit: $ppbv\ h^{-1}$.

acetaldehyde, acetone, propionaldehyde, methyl ethyl ketone, benzaldehyde, and hexanal). Their total mixing ratio was 14.42 ± 3.05 ppbv, accounting for 42% of the measured total VOCs. We assessed the relative contributions of these carbonyls compared with other VOCs using RIR analysis. The results indicated the dominant role of carbonyls in O_3 formation, and formaldehyde was the largest contributor among the individual species.

The formation of O_3 and RO_x (OH , HO_2 , and RO_2) radicals were studied in detail base on OBM-AOCP simulations. Zero-out sensitivity studies showed that 37% of peak net O_3 production rates could be attributed to the presence of carbonyls. This was mainly caused by the large concentration decrease of HO_2 and RO_2 radicals; more than 80% of their primary sources came from photolysis of formaldehyde and other oxygenated VOCs. As both primary and secondary sources may contribute significantly to the concentrations of carbonyls in the urban areas (Chen et al., 2014; Qian et al., 2019; Zhang et al., 2013), it is essential to identify their dominant sources in the future to carry out collaborative control for the regulation of urban O_3 pollution, which has become a significant air quality issue in China.

CRediT authorship contribution statement

Hengqing Shen: Conceptualization, Formal analysis, Writing – original draft. **Yuhong Liu:** Formal analysis, Data curation. **Min Zhao:** Conceptualization, Investigation. **Juan Li:** Supervision, Writing – review

& editing. **Yingnan Zhang:** Investigation, Data curation. **Juan Yang:** Investigation. **Ying Jiang:** Data curation. **Tianshu Chen:** Data curation. **Miao Chen:** Resources. **Xianbing Huang:** Resources. **Chengliu Li:** Investigation, Resources. **Danling Guo:** Resources. **Xiaoyan Sun:** Resources. **Likun Xue:** Conceptualization, Funding acquisition, Project administration, Writing – review & editing. **Wenxing Wang:** Supervision, Resources.

Declaration of competing interest

The authors declare that they have no known competing financial interests or personal relationships that could have appeared to influence the work reported in this paper.

Acknowledgments

This work was funded by Shandong Provincial Science Foundation for Distinguished Young Scholars (ZR2019JQ09), the National Natural Science Foundation of China (41922051), and the Jiangsu Collaborative Innovation Center for Climate Change, and major projects for people's livelihood from Jinan Science and Technology Bureau (201807008). We thank the MCM group of the University of Leeds for providing the MCM model and the National Center for Atmospheric Research for providing the TUV model.

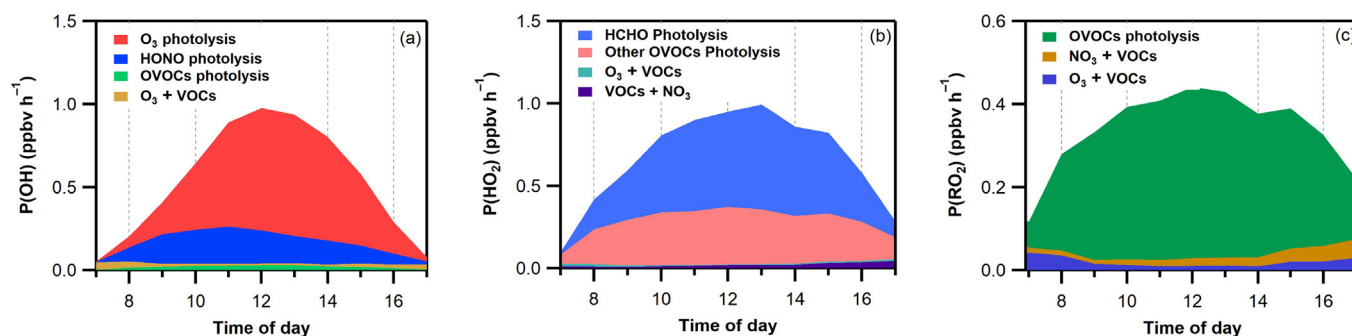


Fig. 7. Primary daytime production rates of (a) OH , (b) HO_2 , and (c) RO_2 radicals during the selected episodes. The OVOCs here include the measured carbonyls other than formaldehyde and modeled OVOCs.

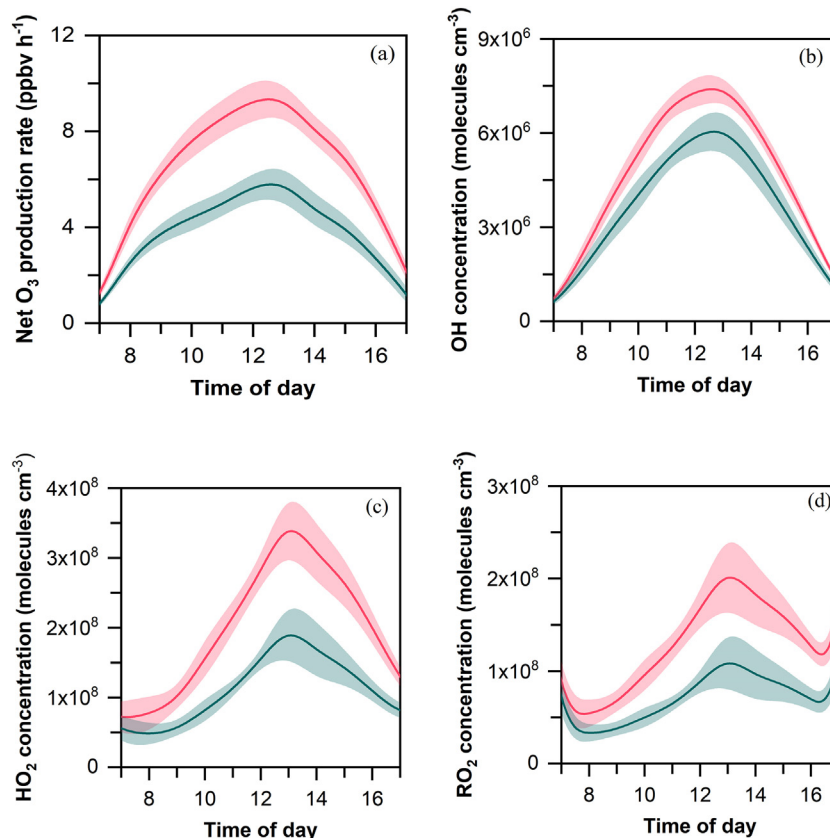


Fig. 8. Model-simulated results of (a) net O₃ production rate, (b) OH, (c) HO₂, and (d) RO₂ radicals with (red) or without (green) the photochemistry of measured carbonyls during the selected episode. The error bar indicates the standard deviation of the mean.

Appendix A. Supplementary data

Supplementary data to this article can be found online at <https://doi.org/10.1016/j.scitotenv.2020.144031>.

References

- Xue, et al., 2016a. Oxidative capacity and radical chemistry in the polluted atmosphere of Hong Kong and Pearl River Delta region : analysis of a severe photochemical smog episode. *Atmos. Chem. Phys.* 16, 9891–9903.
- Avnery, S., Mauzerall, D.L., Liu, J.F., Horowitz, L.W., 2011. Global crop yield reductions due to surface ozone exposure: 1. Year 2000 crop production losses and economic damage. *Atmos. Environ.* 45, 2284–2296.
- Bloss, C., Wagner, V., Jenkin, M.E., Volkamer, R., Bloss, W.J., Lee, J.D., et al., 2005. Development of a detailed chemical mechanism (MCMv3.1) for the atmospheric oxidation of aromatic hydrocarbons. *Atmos. Chem. Phys.* 5, 641–664.
- Brewer, J.F., Fischer, E.V., Commane, R., Wofsy, S.C., Daube, B.C., Apel, E.C., et al., 2020. Evidence for an oceanic source of methyl ethyl ketone to the atmosphere. *Geophys. Res. Lett.* 47, 10.
- Calvert, J., Mellouki, A., Orlando, J., 2011. *Mechanisms of Atmospheric Oxidation of the Oxygenates*. Oxford University Press.
- Carter, W.P.L., 1994. Development of ozone reactivity scales for volatile organic compounds. *J. Air Waste Manage. Assoc.* 44, 881–899.
- Chen, W.T., Shao, M., Lu, S.H., Wang, M., Zeng, L.M., Yuan, B., et al., 2014. Understanding primary and secondary sources of ambient carbonyl compounds in Beijing using the PMF model. *Atmos. Chem. Phys.* 14, 3047–3062.
- Chen, T., Xue, L., Zheng, P., Zhang, Y., Liu, Y., Sun, J., et al., 2020. Volatile organic compounds and ozone air pollution in an oil production region in northern China. *Atmos. Chem. Phys.* 20, 7069–7086.
- Clifton, O.E., Fiore, A.M., Massman, W.J., Baublitz, C.B., Coyle, M., Emberson, L., et al., 2020. Dry deposition of ozone over land: processes, measurement, and modeling. *Rev. Geophys.* 58, 62.
- Edwards, P.M., Brown, S.S., Roberts, J.M., Ahmadov, R., Banta, R.M., deGouw, J.A., et al., 2014. High winter ozone pollution from carbonyl photolysis in an oil and gas basin. *Nature* 514, 351–354.
- Farmer, D.K., Perring, A.E., Wooldridge, P.J., Blake, D.R., Baker, A., Meinardi, S., et al., 2011. Impact of organic nitrates on urban ozone production. *Atmos. Chem. Phys.* 11, 4085–4094.
- Galbally, I.E., Roy, C.R., 1980. Destruction of ozone at the Earth's surface. *Q. J. R. Meteorol. Soc.* 106, 599–620.
- Garland, J.A., Derwent, R.G., 1979. Destruction at the ground and the diurnal cycle of concentration of ozone and other gases. *Q. J. R. Meteorol. Soc.* 105, 169–183.
- Grosjean, D., Grosjean, E., Gertler, A.W., 2001. On-road emissions of carbonyls from light-duty and heavy-duty vehicles. *Environ. Sci. Technol.* 35, 45–53.
- Hu, W.W., Hu, M., Hu, W., Jimenez, J.L., Yuan, B., Chen, W.T., et al., 2016. Chemical composition, sources, and aging process of submicron aerosols in Beijing: contrast between summer and winter. *J. Geophys. Res.-Atmos.* 121, 1955–1977.
- Jenkin, M.E., Saunders, S.M., Pilling, M.J., 1997. The tropospheric degradation of volatile organic compounds: a protocol for mechanism development. *Atmos. Environ.* 31, 81–104.
- Jenkin, M.E., Saunders, S.M., Wagner, V., Pilling, M.J., 2003. Protocol for the development of the master chemical mechanism, MCM v3 (part B): tropospheric degradation of aromatic volatile organic compounds. *Atmos. Chem. Phys.* 3, 181–193.
- Jenkin, M.E., Young, J.C., Rickard, A.R., 2015. The MCM v3.3.1 degradation scheme for isoprene. *Atmos. Chem. Phys.* 15, 11433–11459.
- Karlsson, P.E., Klingberg, J., Engardt, M., Andersson, C., Langner, J., Karlsson, G.P., et al., 2017. Past, present and future concentrations of ground-level ozone and potential impacts on ecosystems and human health in northern Europe. *Sci. Total Environ.* 576, 22–35.
- Li, L.Y., Xie, S.D., Zeng, L.M., Wu, R.R., Li, J., 2015. Characteristics of volatile organic compounds and their role in ground-level ozone formation in the Beijing-Tianjin-Hebei region, China. *Atmos. Environ.* 113, 247–254.
- Li, D., Xue, L., Wen, L., Wang, X., Chen, T., Mellouki, A., et al., 2018a. Characteristics and sources of nitrous acid in an urban atmosphere of northern China: results from 1-yr continuous observations. *Atmos. Environ.* 182, 296–306.
- Li, J., Chen, X.S., Wang, Z.F., Du, H.Y., Yang, W.Y., Sun, Y.L., et al., 2018b. Radiative and heterogeneous chemical effects of aerosols on ozone and inorganic aerosols over East Asia. *Sci. Total Environ.* 622, 1327–1342.
- Li, K., Jacob, D.J., Liao, H., Shen, L., Zhang, Q., Bates, K.H., 2019. Anthropogenic drivers of 2013–2017 trends in summer surface ozone in China. *Proc. Natl. Acad. Sci. U. S. A.* 116, 422–427.
- Li, Q.Q., Su, G.J., Li, C.Q., Liu, P.F., Zhao, X.X., Zhang, C.L., et al., 2020. An investigation into the role of VOCs in SOA and ozone production in Beijing, China. *Sci. Total Environ.* 720, 14.
- Liu, Z., Wang, Y., Gu, D., Zhao, C., Huey, L.G., Sticker, R., et al., 2012. Summertime photochemistry during CAREBeijing-2007: RO_x budgets and O₃ formation. *Atmos. Chem. Phys.* 12, 7737–7752.

- Lu, K., Zhang, Y., Su, H., Brauers, T., Chou, C.C., Hofzumahaus, A., et al., 2010. Oxidant ($O_3 + NO_2$) production processes and formation regimes in Beijing. *J. Geophys. Res.* 115, 18.
- Lu, K.D., Rohrer, F., Holland, F., Fuchs, H., Bohn, B., Brauers, T., et al., 2012. Observation and modelling of OH and HO_2 concentrations in the Pearl River Delta 2006: a missing OH source in a VOC rich atmosphere. *Atmos. Chem. Phys.* 12, 1541–1569.
- Lu, X., Hong, J.Y., Zhang, L., Cooper, O.R., Schultz, M.G., Xu, X.B., et al., 2018. Severe surface ozone pollution in China: a global perspective. *Environ. Sci. Technol. Lett.* 5, 487–494.
- Lu, H.X., Lyu, X.P., Cheng, H.R., Ling, Z.H., Guo, H., 2019a. Overview on the spatial-temporal characteristics of the ozone formation regime in China. *Environ. Sci. Process. Impacts* 21, 916–929.
- Lu, K., Fuchs, H., Hofzumahaus, A., Tan, Z., Wang, H., Zhang, L., et al., 2019b. Fast photochemistry in wintertime haze: consequences for pollution mitigation strategies. *Environ. Sci. Technol.* 53, 10676–10684.
- Malley, C.S., Henze, D.K., Kuylenstierna, J.C.I., Vallack, H.W., Davila, Y., Anenberg, S.C., et al., 2017. Updated global estimates of respiratory mortality in adults ≥ 30 years of age attributable to long-term ozone exposure. *Environ. Health Perspect.* 125, 9.
- Mellouki, A., Wallington, T.J., Chen, J., 2015. Atmospheric chemistry of oxygenated volatile organic compounds: impacts on air quality and climate. *Chem. Rev.* 115, 3984–4014.
- Mills, G., Sharps, K., Simpson, D., Pleijel, H., Broberg, M., Uddling, J., et al., 2018. Ozone pollution will compromise efforts to increase global wheat production. *Glob. Chang. Biol.* 24, 3560–3574.
- Nogueira, T., de Souza, K.F., Fornaro, A., Andrade, M.D., de Carvalho, L.R.F., 2015. On-road emissions of carbonyls from vehicles powered by biofuel blends in traffic tunnels in the Metropolitan Area of Sao Paulo, Brazil. *Atmos. Environ.* 108, 88–97.
- Ojha, N., Naja, M., Singh, K.P., Sarangi, T., Kumar, R., Lal, S., et al., 2012. Variabilities in ozone at a semi-urban site in the indo-Gangetic plain region: association with the meteorology and regional processes. *J. Geophys. Res.-Atmos.* 117, 19.
- Qian, X., Shen, H., Chen, Z., 2019. Characterizing summer and winter carbonyl compounds in Beijing atmosphere. *Atmos. Environ.* 214, 116845.
- Rao, Z.H., Chen, Z.M., Liang, H., Huang, L.B., Huang, D., 2016. Carbonyl compounds over urban Beijing: concentrations on haze and non-haze days and effects on radical chemistry. *Atmos. Environ.* 124, 207–216.
- Russell, A., Milford, J., Bergin, M.S., McBride, S., McNair, L., Yang, Y., et al., 1995. Urban ozone control and atmospheric reactivity of organic gases. *Science* 269, 491–495.
- Salthammer, T., 2013. Formaldehyde in the ambient atmosphere: from an indoor pollutant to an outdoor pollutant? *Angew. Chem. Int. Ed. Engl.* 52, 3320–3327.
- Saunders, S.M., Jenkin, M.E., Derwent, R.G., Pilling, M.J., 2003. Protocol for the development of the Master Chemical Mechanism, MCM v3 (part A): tropospheric degradation of non-aromatic volatile organic compounds. *Atmos. Chem. Phys.* 3, 161–180.
- Shao, M., Zhang, Y.H., Zeng, L.M., Tang, X.Y., Zhang, J., Zhong, L.J., et al., 2009. Ground-level ozone in the Pearl River Delta and the roles of VOC and NO_x in its production. *J. Environ. Manag.* 90, 512–518.
- Shen, H., Chen, Z., Li, H., Qian, X., Qin, X., Shi, W., 2018. Gas-particle partitioning of carbonyl compounds in the ambient atmosphere. *Environ. Sci. Technol.* 52, 10997–11006.
- Tan, Z.F., Rohrer, F., Lu, K.D., Ma, X.F., Bohn, B., Broch, S., et al., 2018. Wintertime photochemistry in Beijing: observations of RO_x radical concentrations in the North China Plain during the BEST-ONE campaign. *Atmos. Chem. Phys.* 18, 12391–12411.
- Tan, Z., Lu, K., Hofzumahaus, A., Fuchs, H., Bohn, B., Holland, F., et al., 2019a. Experimental budgets of OH, HO_2 , and RO_2 radicals and implications for ozone formation in the Pearl River Delta in China 2014. *Atmos. Chem. Phys.* 19, 7129–7150.
- Tan, Z.F., Lu, K.D., Jiang, M.Q., Su, R., Wang, H.L., Lou, S.R., et al., 2019b. Daytime atmospheric oxidation capacity in four Chinese megacities during the photochemically polluted season: a case study based on box model simulation. *Atmos. Chem. Phys.* 19, 3493–3513.
- Vermeuel, M.P., Novak, G.A., Alwe, H.D., Hughes, D.D., Kaleel, R., Dickens, A.F., et al., 2019. Sensitivity of ozone production to NO_x and VOC along the Lake Michigan coastline. *J. Geophys. Res. Atmos.* 124, 10989–11006.
- Wang, C., Huang, X.F., Han, Y., Zhu, B., He, L.Y., 2017a. Sources and potential photochemical roles of formaldehyde in an urban atmosphere in South China. *J. Geophys. Res.-Atmos.* 122, 11934–11947.
- Wang, T., Xue, L.K., Brimblecombe, P., Lam, Y.F., Li, L., Zhang, L., 2017b. Ozone pollution in China: a review of concentrations, meteorological influences, chemical precursors, and effects. *Sci. Total Environ.* 575, 1582–1596.
- Wang, H., Wang, Q., Gao, Y., Zhou, M., Jing, S., Qiao, L., et al., 2020a. Estimation of secondary organic aerosol formation during a photochemical smog episode in Shanghai, China. *J. Geophys. Res. Atmos.* 125, e2019JD032033.
- Wang, Y., Gao, W., Wang, S., Song, T., Gong, Z., Ji, D., et al., 2020b. Contrasting trends of $PM_{2.5}$ and surface-ozone concentrations in China from 2013 to 2017. *Nat. Sci. Rev.* 7, 1331–1339.
- Wollenhaupt, M., Carl, S.A., Horowitz, A., Crowley, J.N., 2000. Rate coefficients for reaction of OH with acetone between 202 and 395 K. *J. Phys. Chem. A* 104, 2695–2705.
- Wu, R., Li, J., Hao, Y., Li, Y., Zeng, L., Xie, S., 2016. Evolution process and sources of ambient volatile organic compounds during a severe haze event in Beijing, China. *Sci. Total Environ.* 560–561, 62–72.
- Wu, W., Zhao, B., Wang, S., Hao, J., 2017. Ozone and secondary organic aerosol formation potential from anthropogenic volatile organic compounds emissions in China. *J. Environ. Sci.* 53, 224–237.
- Xue, L.K., Wang, T., Guo, H., Blake, D.R., Tang, J., Zhang, X.C., et al., 2013. Sources and photochemistry of volatile organic compounds in the remote atmosphere of western China: results from the Mt. Waliguan Observatory. *Atmos. Chem. Phys.* 13, 8551–8567.
- Xue, L.K., Wang, T., Gao, J., Ding, A.J., Zhou, X.H., Blake, D.R., et al., 2014. Ground-level ozone in four Chinese cities: precursors, regional transport and heterogeneous processes. *Atmos. Chem. Phys.* 14, 13175–13188.
- Xue, L., Gu, R., Wang, T., Wang, X., Saunders, S., Blake, D., et al., 2016b. Oxidative capacity and radical chemistry in the polluted atmosphere of Hong Kong and Pearl River Delta region: analysis of a severe photochemical smog episode. *Atmos. Chem. Phys.* 16, 9891–9903.
- Yang, X., Xue, L., Wang, T., Wang, X., Gao, J., Lee, S., et al., 2018. Observations and explicit modeling of summertime carbonyl formation in Beijing: identification of key precursor species and their impact on atmospheric oxidation chemistry. *J. Geophys. Res. Atmos.* 123, 1426–1440.
- Yang, J., Shen, H., Guo, M.-Z., Zhao, M., Jiang, Y., Chen, T., et al., 2021. Strong marine-derived nitrous acid (HONO) production observed in the coastal atmosphere of northern China. *Atmos. Environ.* 244, 117948.
- Zhang, Y.L., Cao, F., 2015. Fine particulate matter ($PM_{2.5}$) in China at a city level. *Sci. Rep.* 5, 14884.
- Zhang, H.L., Li, J.Y., Ying, Q., Guven, B.B., Olaguer, E.P., 2013. Source apportionment of formaldehyde during TexAQ5 2006 using a source-oriented chemical transport model. *J. Geophys. Res.-Atmos.* 118, 1525–1535.
- Zhang, Y.N., Xue, L.K., Dong, C., Wang, T., Mellouki, A., Zhang, Q.Z., et al., 2019. Gaseous carbonyls in China's atmosphere: tempo-spatial distributions, sources, photochemical formation, and impact on air quality. *Atmos. Environ.* 214, 15.
- Zhang, G., Xu, H.H., Wang, H.L., Xue, L.K., He, J.J., Xu, W.Y., et al., 2020a. Exploring the inconsistent variations in atmospheric primary and secondary pollutants during the 2016 G20 summit in Hangzhou, China: implications from observations and models. *Atmos. Chem. Phys.* 20, 5391–5403.
- Zhang, K., Li, L., Huang, L., Wang, Y., Huo, J., Duan, Y., et al., 2020b. The impact of volatile organic compounds on ozone formation in the suburban area of Shanghai. *Atmos. Environ.* 232, 117511.
- Zheng, B., Tong, D., Li, M., Liu, F., Hong, C.P., Geng, G.N., et al., 2018. Trends in China's anthropogenic emissions since 2010 as the consequence of clean air actions. *Atmos. Chem. Phys.* 18, 14095–14111.
- Zhu, B., Han, Y., Wang, C., Huang, X.F., Xia, S.Y., Niu, Y.B., et al., 2019. Understanding primary and secondary sources of ambient oxygenated volatile organic compounds in Shenzhen utilizing photochemical age-based parameterization method. *J. Environ. Sci.* 75, 105–114.